Received: 27 February 2021 | Revised: 3 June 2021 | Accepted: 3 June 2021

DOI: 10.1002/jrs.6178

SPECIAL ISSUE - INVITED REVIEW

Journal of RAMAN SPECTROSCOPY WILEY

Raman spectroscopy and correlative-Raman technology excel as an optimal stage for carbon-based electrode materials in electrochemical energy storage

Ying Zheng[1] | Ting Deng[1] | Nailin Yue[1] | Wei Zhang[1,2,3,4] | Xuanbo Zhu[1,2] | He Yang[1] | Xianyu Chu[1] | Weitao Zheng[1]

[1]State Key Laboratory of Automotive Simulation and Control, and School of Materials Science & Engineering, Electron Microscopy Center, and International Center of Future Science, Jilin University, Changchun, 130012, China

[2]National and Local Joint Engineering Laboratory for Synthetic Technology of High Performance Polymer, College of Chemistry, Jilin University, Changchun, 130012, China

[3]Wuhan National Laboratory for Optoelectronics, Huazhong University of Science and Technology, Wuhan, 430074, China

[4]IKERBASQUE, Basque Foundation for Science, Bilbao, 48013, Spain

Correspondence
Wei Zhang, State Key Laboratory of Automotive Simulation and Control, and School of Materials Science & Engineering, Electron Microscopy Center, and International Center of Future Science, Jilin University, Changchun 130012, China.
Email: weizhang@jlu.edu.cn

Xuanbo Zhu, National and Local Joint Engineering Laboratory for Synthetic Technology of High Performance Polymer, College of Chemistry, Jilin University, Changchun 130012, China.
Email: zhuxuanbo@jlu.edu.cn

Weitao Zheng, State Key Laboratory of Automotive Simulation and Control, and School of Materials Science & Engineering, Electron Microscopy Center, and International Center of Future Science, Jilin University, Changchun 130012, China.
Email: wtzheng@jlu.edu.cn

Funding information
National Natural Science Foundation of China, Grant/Award Number: 51932003, 51872115; Fundamental Research Funds for the Central Universities; Open Project Program of Wuhan National Laboratory for Optoelectronics, Grant/Award Number: 2018WNLOKF022; Jilin Province/Jilin University Co-construction Project Funds for New Materials, Grant/Award Numbers: Branch-

Abstract

The structural details of carbon materials directly affect their properties as an electrode material, such as specific capacitance and coulomb efficiency. Therefore, the structural analysis of carbon materials has always been an important step in the mechanistic insight into their roles in electrochemical energy storage. Raman spectroscopy, as molecular spectroscopy technique, has been widely used in understanding the lattice vibration mechanics of carbon materials and providing information on the chemical structure at molecular level, as well as microstructure analysis of carbon materials. In addition, the development of correlative-Raman technology enables clarifying more comprehensive and accurate structural information for carbon-based materials. With this information, it is of great significance to guide the construction of advanced carbon-based electrode materials for energy storage.

KEYWORDS

carbon-based materials, in situ electrochemistry, Raman imaging and secondary electron microscopy (RISE)

2/440050316A36, SXGJSF2017-3; China Postdoctoral Science Foundation, Grant/Award Number: 2020M670838; National Postdoctoral Program for Innovative Talents, Grant/Award Number: BX20200147; Project for Self-innovation Capability Construction of Jilin Province Development and Reform Commission, Grant/Award Number: 2021C026; Program for the Development of Science and Technology of Jilin Province, Grant/Award Number: 20190201309JC; Department of Science and Technology of Jilin Province, Grant/Award Number: 20200801001GH

1 | INTRODUCTION

Carbon materials have been widely used in electrochemical energy storage electrode materials because of their advantages such as abundance, good electrical conductivity, good stability, non-toxic, and pollution-free features.[1] Raman spectroscopy has been widely used in biology,[2,3] medicine,[4] and archaeology.[5] Raman peak intensity provides information about concentration and molecular orientation (polarization); the peak position of Raman spectrum clarifies the information of functional groups and structure; the peak displacement reflects the possible stress/strain and pressure; the information of defect, doping, and crystallinity can be obtained by analyzing half height width; Raman peak ratio corresponds to the relative intensity information.[6–8] In addition, Raman spectroscopy has the advantages of fast, nondestructive, non-contact, and high spatial resolution.[9] Raman spectroscopy plays an irreplaceable role in investigations of carbon materials.[10] Ajayan et al.[11] summarized the reports of some carbon materials involved with Raman spectroscopy in the last 30 years (based on Web of Science). Raman spectroscopy has been increasingly used for common carbon materials such as graphite, graphene, carbon nanotubes, and carbon fiber and has thereof attracted more and more attention.

Supercapacitors[12,13] and lithium-ion batteries,[14–16] as the typical electrochemical energy storage devices, are very important for storage and conversion of new energy.[17] Carbon materials are widely used as electrode materials for batteries and supercapacitors due to their high conductivity, stability, non-toxicity, wide source, good stability, and diversity. The structural details of carbon material directly affect their performance as electrode materials. For example, as graphite has obvious regular layer structure, it can be used as an active electrode material for batteries, allowing ions to be intercalated and deintercalated between graphite layers for charge storage,[18] whereas the carbon fiber has a disordered layer graphite structure, usually used as the electrode active material for supercapacitors, where charges is stored via double electric layers.[19] To obtain high power density and energy density energy storage devices, electrode active materials are usually required with high specific capacitance, wide potential window, and long cycle life. To improve these performances of carbon-based electrode materials, it often requires comprehensive understanding of the energy storage mechanism[20,21] and continuous optimization of the surface/interface structure.[22–24] Raman spectroscopy provides very important information for the optimization of carbon-based electrode materials. For instance, it enables clarifying the degree of graphitization and surface functional groups of carbon materials. The higher the graphitization degree represents, the more conducive to the intercalating of ions between graphite layers; pseudocapacitance may be introduced due to surface functional groups of carbon materials.

Moreover, correlative-Raman technology has been recently developed. It can provide information on various aspects of materials and achieve accurate analysis. As is known, the integration of Raman-SEM,[25] Raman-SEM–EDX,[26] and Raman-AFM[27,28] can afford a variety of comprehensive details in the same micro-regions, with which very accurate and effective information are provided for analysis of electrode material structure. Since the electrode active materials change dynamically in the process of energy storage and conversion, they often need to be analyzed in real-time. The in situ electrochemical Raman spectroscopy combined by Raman spectroscopy and electrochemical cell makes up for this need.[29] The structural change of electrode materials can be thereof recorded during charging and discharging process, which facilitates clarifying the energy storage mechanism of materials.[30] Compared to the individual characterization techniques, such correlative-Raman techniques are superior.

In this review, the application and potential of Raman spectroscopy in the research of carbon-based energy storage electrode materials are reviewed. Our paper briefly reviewed the principle of Raman's research on carbon materials and summarized the application of Raman spectroscopy in carbon materials with different energy storage mechanisms. We put forward the advantages of some advanced correlative-Raman techniques in the research field of energy storage electrode materials. As a consequence, it proves that Raman spectroscopy has a very high potential in the study of carbon-based energy storage electrode materials.

2 | THE PRINCIPLE OF RAMAN SPECTROSCOPY

The Raman effect was predicted by physicist Smekal,[31] until physicist C.V. Raman discovered that the wavelength of an incident light is different from the one of the scattered light. Since then, the scattered light that has a different wavenumber from the incident light is called Raman scattering, and the displacement of the wavenumber is named Raman shift.[32,33] Raman activity depends on whether a molecular polarization changes when the molecule vibrates; that is, only the molecular vibration mode with the change of molecular polarization can produce Raman scattering. The magnitude of Raman shift is not correlated with the excitation energy but is only related to the molecular energy level structure. Thus, the Raman shift can reflect the molecular vibration wavenumber or rotational wavenumber. Because the materials with different molecular structures have different energy level structures, they have different Raman shifts, Raman lines, and Raman relative strengths. This is the basis of qualitative analysis of molecular groups and molecular structures. For the same materials, Raman scattering intensity is proportional to group content. It is challenging to measure conventional Raman spectroscopy because of its weak signals. It has been one of the research directions of Raman spectroscopy to continuously improve the measurement method based on the original techniques. For example, resonance Raman spectroscopy (When the laser wavenumber approaches the electron absorption wavenumber of an object, the laser photon energy is comparable to the energy of an electron transition; As a result of such resonance, the increase of Raman scattering intensity will occur by 10^2–10^6 times),[34,35] Fourier transform Raman spectroscopy (The integrating the near-infrared excitation Raman technique and Fourier transform technique),[36] microscopic confocal Raman spectroscopy (The Raman spectrometer is combined with a standard light microscope; the laser beam is focused through a microscope into a spot with a diameter of 0.5–1.0 μm; Then, the Raman signal in a spot passes through the microscope and travels back to the spectrometer, where the spectral information is obtained),[37] and surface enhanced Raman spectroscopy (It is an surface enhanced effect associated with rough surfaces; Only three kinds of metals, viz., gold, silver, copper, and a few uncommon alkali metals [such as lithium and sodium] have strong surface enhanced effect; It is only after surface coarsening that gold, silver, and copper will have high surface enhanced activities)[3,38] are being developed and flourished.

The characterization and analysis of carbon materials by Raman spectroscopy have formed a complete theoretical system. The large family of carbon materials can be divided into sp^1, sp^2, and sp^3 carbon materials.[39] Most of these sp^2 carbon materials can be thought of as evolved from a single layer of graphene. Single-layer graphene is sp^2 carbon atoms that tightly packed two-dimensional atomic crystal possess hexagonal honeycomb structure.[40] A protocell contains two non-equivalent carbon atoms A and B, and there are six phonon dispersion curves, namely, the in-plane longitudinal optical (iLO), in-plane transverse optical (iTO) and out-plane transverse optical (oTO), in-plane longitudinal acoustic (iLA), in-plane transverse acoustic (iTA), and out-plane transverse acoustic (oTA).[41] There are four characteristic peaks in a typical Raman spectra of graphene edge. The G-peak (1,582 cm^{-1}) is generated by the in-plane vibration of the sp^2 carbon atom, which is due to the doubly degenerated iTO and iLO optical phonon interaction in the center of the Brillouin region. G peak has E_{2g} symmetry and is the only first-order Raman scattering process in monolayer graphene. The 2D peak (2,700 cm^{-1}) is generated by two valley inelastic scattering with the iTO optical phonon near the K point, while the D peak (1,350 cm^{-1}) involves valley scattering between an iTO phonon and a defect. The D′ peak (~1,620 cm^{-1}) is the double resonance process in the valley, and the two scattering processes are the intra-valley scattering of the defect and the inelastic intra-valley scattering of the iLO phonon near the Gamma point, respectively.[42] The Raman spectrum analysis of carbon materials is mainly based on these four peaks.

3 | CARBON-BASED ELECTROCHEMICAL ENERGY STORAGE ELECTRODE MATERIALS

The basic requirement of carbon-based materials as electrochemical energy storage electrode materials is good electrical conductivity. The most common carbon

materials in electrochemical energy storage electrode materials include high purity graphite,[43,44] expanded graphite,[18] carbon nanomaterials (such as graphene[45] and carbon nanotubes),[46] carbon fiber,[19] and activated carbon.[47] Carbon materials have more complex surface chemical structures than metallic materials. This is because carbon materials abounds in a variety of structures, surface bonds and functional groups.[48] The energy storage mechanism of carbon materials can be roughly divided into two kinds: the electrical double layer mechanism and intercalation/de-intercalation mechanism. Raman spectroscopy has different advantages for these two types of energy storage carbon materials.

3.1 | Electrical double layer mechanism

Carbon materials with the electrical double layer energy storage mechanism are commonly found in supercapacitors.[49] Charged ions are adsorbed on the surface of carbon materials through electrostatic action to form a compact double layer for charge storage. The electrical double layer is divided into three parts: the inner Helmholtz layer (IHP), the outer Helmholtz layer (OHP) and the diffuse layer. The diffuse layer is caused by the thermal movement of ions, which is only correlated to the temperature, concentration and the residual charge density of the diffuse layer. The non-special ion adsorption of OHP is mainly electrostatic adsorption through a coulomb interaction. Whereas IHP has special ion adsorption. In general, most inorganic cations do not undergo special adsorption, except for only a few cations with low hydration energy (e.g., Cs^+) that can make. However, such special adsorption will more or less occur for almost all anions. For this kind of carbon-based electrode materials, the methods to improve the specific capacitance include optimizing the electrical conductivity, increasing the specific surface area, constructing hierarchical pore structure[50] and introducing pseudocapacitance.

Some work on the characterization of carbon-based supercapacitor energy storage electrode materials by Raman spectroscopy are listed in Table S1 (Supporting Information). ID/IG is treated as one of the parameters for the carbon electrodes. For example, Ferrari et al.[51] pointed out that for a definite L_D (the distance between defects), ID/IG depends on the laser energy. A set of empirical relations (satisfied under specific conditions) was thereof proposed to quantitatively analyze point defects in graphene using Raman spectroscopy. In another work, they described the detailed Raman spectra from graphite to tetrahedral amorphous carbon.[52] A three-stage model is proposed: First, graphite is converted to nanocrystalline graphite, and then the latter to low-sp^3 amorphous carbon, and finally to high-sp^3 amorphous carbon. The defects affect largely the specific capacitance in the double-layer supercapacitor electrodes. Chen et al.[53] revealed how the inclusion of topological defects or heterogeneous atoms in graphene can lead to the capacitance increase of an electrical double layer. That is, the defects increase the density of electronic state (DOS) of carbon materials, i.e., an increase of the quantum capacitance. On the other hand, heterogeneous atom doping enables mainly the changes of the Fermi level, and its effect on the electron density of states is relatively negligible. However, both of them affect quantum capacitors in series with Helmholtz capacitors, thereby resulting in an alternation of the electrical double layer capacitors. Although there are more defects (a larger ID/IG in Table S1), no larger specific capacitance can be found. This is because the specific capacitance of carbon materials is related not only to defects but also to specific surface area, morphology, and other factors. For example, Wang et al.[54] used a nitrogen atmosphere to activate carbon fiber cloth at different temperatures. ID/IG gradually increases with the annealing temperature (Figure 1a), indicating an increase of surface disorder (increasing defects) and the specific capacitance increased gradually (Figure 1d). This is because the specific surface area increases with the increase of annealing temperature, which is conducive to the formation of double electric layer (Figure 1b). At the same time, the decrease of contact angle (from hydrophobic characteristics to super-hydrophilic characteristics) is beneficial to the contact between electrode and electrolyte (Figure 1c). Therefore, the evaluation of the overall performance of the electrode should be combined with a variety of characterization techniques.

Due to the limitations of carbon materials, such as low specific capacity (the specific capacitance of carbon has been at a moderate level of 100–200 F/g for decades [19]), they are usually compounded with other materials to improve the specific capacitance of the electrode.[55–57] Raman spectroscopy can not only analyze the defects of carbon-based composite electrode materials but also analyze the types of materials and play a role in phase identification. Chen et al.[58] prepared porous α-Fe_2O_3 nanorods and carbon nanotube-graphene foam composites. The process diagram is shown in Figure S2a–c. First, graphene foam (GF) was prepared. Carbon nanotubes were then grown on graphene foam (CNT-GF); finally, Fe_2O_3/CNT-GF was prepared by solvent heating and annealing methods. XRD (Figure S2h) and SEM (Figure S2d–f) were used to analyze the synthesized products of each step and their corresponding morphologies. The test results of Raman are shown in Figure S2g. The characteristic peaks at 227, 290, 408, and 607 cm^{-1}

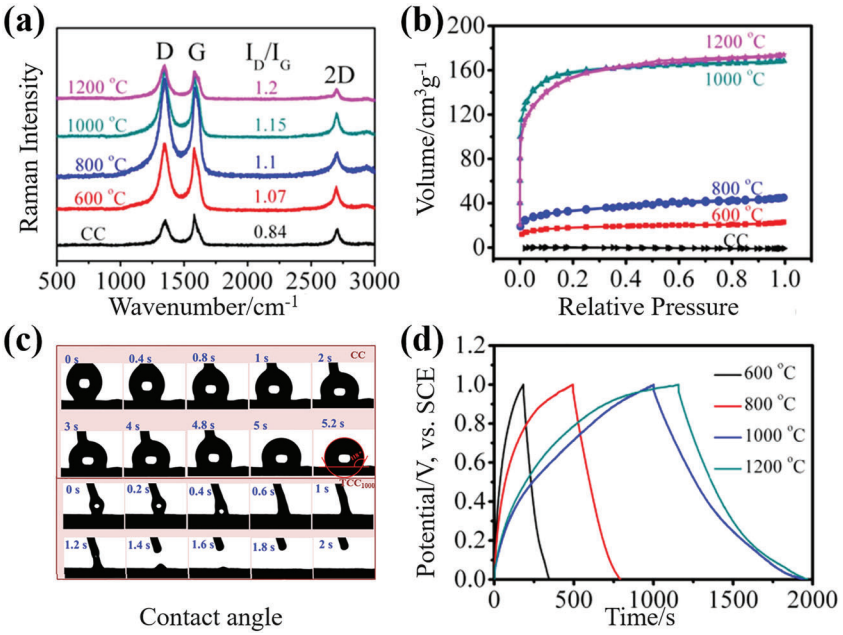

FIGURE 1 (a–d) Raman spectra test diagrams, nitrogen adsorption/desorption test diagrams, contact angle test diagrams, and galvanostatic discharge-charge diagrams of carbon cloth and activated carbon cloth, respectively. This figure was reprinted with permission from Wang et al.[54] Copyright 2017 Elsevier BV [Colour figure can be viewed at wileyonlinelibrary.com]

belong to the A_{1g} and E_g modes of α-Fe_2O_3. The characteristic peak at 1,313 cm^{-1} is the double magnon scattering peak. CNT-GF only exists in D-band and G-band. It can be seen from the Raman spectrum of the composite electrode material that there is an obvious characteristic peak of Fe_2O_3. It was proved that Fe_2O_3 and CNT-GF are composited successfully. Guo et al.[59] also analyzed the structure of Co–Fe_3O_4 NS@NG (cobalt encapsulated Fe_3O_4 nanosphere is developed on N-graphene sheet) by Raman spectroscopy. The Raman characteristic peak of Fe_3O_4 (≈200–800 cm^{-1}) showed that the complex was successfully synthesized. At the same time, it proved that Co-doping is beneficial to curing of the structural imperfections through modifying ID/IG.

3.2 | Intercalation/de-intercalation mechanism

Carbon materials with intercalation/de-intercalation mechanism are commonly found in battery systems. Taking a dual-ion battery as an example, the energy storage process is shown in Figure S1a,b.[60] The anions and cations in the electrolyte are intercalated into the cathode and anode respectively during charging. During discharge, the anions/cations are removed from the cathode/anode and returned to the electrolyte. Such carbon materials often have a distinct layer structure of graphite that allows charged ions to be intercalated to form acceptor-type graphite-intercalated compounds (GIC).[61, 62] Taking the formation of GIC by anions intercalated in graphite cathode as an example, there is a large height between the carbon planes of GIC. That is, the interaction between the layers is weakened. Therefore, the anions intercalating into the graphite electrode is usually accompanied by a large volume expansion. In addition, the complex electrostatic and elastic interactions between anions affect the subsequent anions intercalation dynamics and the storage capacity of anions.[63] Placke et al.[64] systematically studied the intercalation behavior of graphite with a series of anions, including PF_6^-, BF_4^-, $TFSI^-$, and $FTFSI^-$. The degree of anion intercalating is positively correlated with specific capacity during charging. The degree of intercalating of ions is usually marked by stage. The definition of stage is based on the assumption that a continuous GIC is formed in a defect-free graphite lattice.[65] It is described in terms of the number of graphene layers inserted between adjacent ionic layers,[66] for example, the number 4 corresponding to stage 4. Raman spectroscopy is very sensitive to the change of graphite structure. When the ions are intercalated into the graphite, the G band of the graphite is blue shifted and split into two mode, inner ($E_{2g(i)}$) and outer ($E_{2g(b)}$).[67–69] Based on $IE_{2g(i)}$ and $IE_{2g(b)}$, we can calculate the number of intercalation stage.[70] Formula is as follows:

$$\frac{I_i}{I_b}=\frac{\sigma_i}{\sigma_b}\frac{(n-2)}{2},$$

where σ_i/σ_b represents the ratio of Raman scattering cross sections of the inner and the boundary carbon layers and suggested that this ratio is a unity in case of lithium intercalation.[71] This n represents the intercalation stage ($n > 2$).

Angell et al.[72] used Raman spectroscopy to study the structural changes of graphite during charge and discharge in aluminum ion batteries. Figure 2a,b shows the Raman spectrum of the intercalation process and the constant current charging curve. The original graphite has G peak at 1,584 cm^{-1}, and the G peak is shifted by 20 cm^{-1} under the lower charging platform, thus generating two different E_{2g} peaks. This is due to the rearrangement of positive charges on the graphite boundary layer caused by anion intercalation. At 1.94–1.99 V charging platform (Raman spectrum green line), $E_{2g(b)}$ underwent a small split. In this case, n is approximately equal to 2.5. Then, $E_{2g(i)}$ disappears after continuous charging, and $E_{2g(b)}$ intensity increases. Continue charging to 2.097–2.3 V. $E_{2g(b)}$ has a large splitting at 1,619–1,632 cm^{-1}. In the fully charged state, only one high-intensity peak of 1,632 cm^{-1} still exists, indicating that stage 1 or 2 GIC is formed because neither $E_{2g(i)}$ nor $E_{2g(b)}$ bands exist. The de-intercalation process is shown in Figure 2c,d. The discharge process is a reversible reaction of the charging process, and Raman spectrum has the opposite result. Raman spectroscopy proves the structural changes of graphite at different potentials during charging and discharging, which is helpful to understand the specific reaction process of the formation of graphite-intercalated compounds by ions intercalation into graphite. Shi et al.[73] also used this method to study the structural changes of carbon fiber paper cathode when PF_6^- intercalated into cathode in the dual-ion battery. Kim et al.[74] used graphite as cathode material for aqueous dual-ion batteries and magnesium chloride and choline as water-in-salt electrolyte. XRD showed that no new compounds were formed when Mg-Cl superhalides were inserted into graphite. Combined with Raman spectra, the G peak does not split under full charging condition, indicating that the insertion of Mg-Cl superhalide does not form GIC but only leads to the defects generated during cycling. Combined with the results of ex situ high-resolution transmission electron microscopy, it is believed that the anion intercalation process induces turbostratic structural sites. This result is of great significance for the future research of carbon-based-aqueous dual-ion batteries battery. However, Zhang et al.[75] used graphite as the cathode of aqueous dual-ion batterie, 21 M of LiTSI, and 3 M of $ZnTfO_2$ as the electrolyte. It leads to the formation of a diversity of stages at different charging potentials. Raman spectroscopy plays an irreplaceable role in the study of anions intercalated behaviors in graphite. Therefore, the Raman spectroscopy of GICs has been widely explored.[76–78]

4 | ADVANCED CORRELATIVE-RAMAN TECHNOLOGY

With the development of research on electrode materials, it is often required to conduct more in-depth testing and analysis in order to obtain more comprehensive and effective information and optimize the electrode continuously. Especially, testing the electrode in the electrode reaction process is usually required, such as in situ XRD technology.[79] Raman spectroscopy has some limitations in the study of carbon-based electrodes. It can only acquire information about the chemical structure of the surface. Therefore, it is very important for the development of correlative-Raman technology. Raman

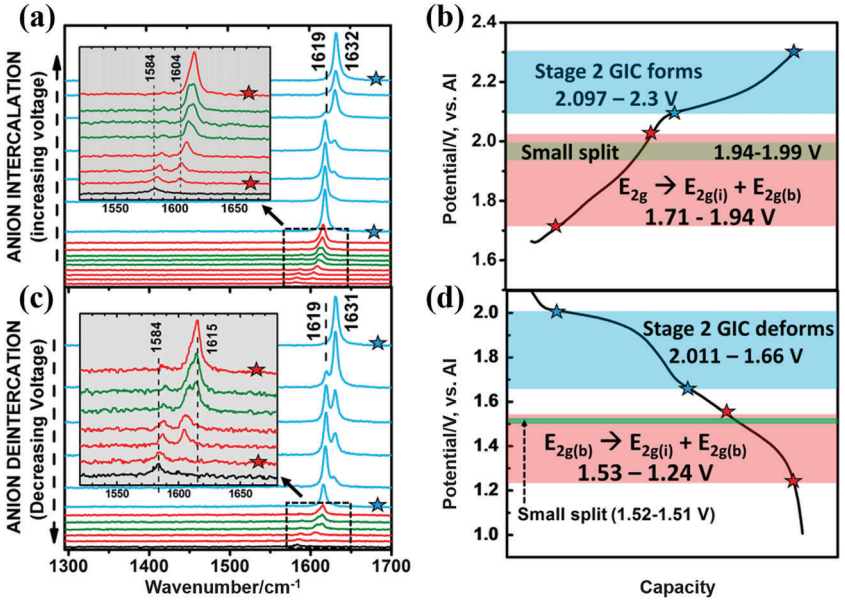

FIGURE 2 (a and c) Raman spectra of the charging and discharging processes, respectively. (b and d) Galvanostatic discharge-charge curves of the corresponding processes. This figure was reprinted with permission from Angell et al.[72] Copyright the authors and 2017 National Academy of science [Colour figure can be viewed at wileyonlinelibrary.com]

spectroscopy combined with other characterization techniques to obtain more accurate and rich information, which is also one of the future development directions of Raman spectroscopy. For example, Raman spectroscopy is used in combination with electron microscopy and electrochemical measurement (galvanostatic charge-discharge[12] and capillary electrophoresis[80]).

4.1 | Raman-SEM

RISE (Raman Imaging and Secondary Electron Microscopy) technology was successfully established in 2014,[81] combining Raman and scanning electron microscopy (SEM). Figure 3 shows the correlative SEM-Raman equipment using a TESCAN S9000G electron microscope integrated with a WITec R300 confocal Raman imaging system at Electron Microscopy Center of Jilin University. Confocal Raman microscopes are placed in the vacuum chamber of the electron microscope and controlled directly by RISE software. Raman and scanning electron microscopy measurements are carried out continuously at two different locations in this chamber using the automatic transfer stage. The position shown in Figure 3a is Raman measurement, and the position shown in Figure 3b is SEM measurement. RISE uses a carefully calibrated piezoelectric scanning technique to ensure that the same area of the sample is scanned in SEM and Raman modes. By superimposing Raman surface image and SEM image according to a different mixing degree, RISE image containing both SEM morphology information and Raman information can be obtained.

For example, graphene films are grown on silicon substrate by CVD, and SEM images of graphene films are obtained by RISE test.[81] SEM shows sheets of graphene growing on the substrate. More detailed characterization of graphene films by confocal Raman spectroscopy: the defects in graphene films lead to differences in peak width and peak strength in Raman spectra. Several graphene layers may be distinguished according to the difference in 2D peak. In the RISE image, single-layer graphene regions (blue), and multi-layer graphene regions (green and red) are shown. The silicon substrate is shown in yellow, and this test method well explains the layer structure information of different regions of the graphene films. In this way, the morphology of the deposited graphene films and the corresponding films thickness can be known simultaneously. In addition, RISE can be also used in conjunction with EDX to obtain the chemical structure information, elemental distribution information, and surface morphology information in the same microregion.[26, 83]

RISE has great advantages in the characterization of electrode materials [84]. The surface morphology and chemical structure information are measured separately in the traditional testing process. The RISE technology can be used to characterize the morphology and chemical structure in the same microregion, which is very important for electrode optimization and design. Zheng et al.[82] also used RISE technology to explore the surface

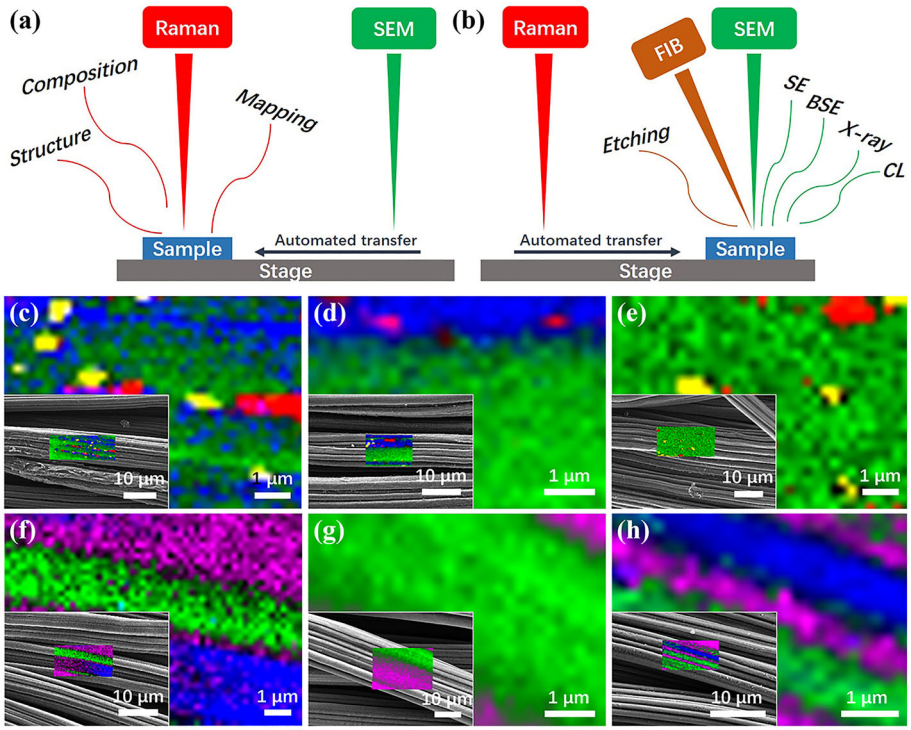

FIGURE 3 Schematic diagram of correlative SEM-Raman (RISE microscopy) equipment at Electron Microscopy Center of Jilin University. (a) Raman spectroscopic mode; (b) SEM mode. (c–h) Raman images of CFC, 350CFC, 400CFC 425CFC, 450CFC, and 475CFC, respectively. The insets are the corresponding RISE images. This figure was reprinted with permission from Zheng et al.[82] Copyright 2020 Elsevier BV [Colour figure can be viewed at wileyonlinelibrary.com]

structure and corresponding chemical information of carbon fiber cloth (CFC) electrode. The activated commercial CFCs were marked as 350CFC, 400CFC, 425CFC, 450CFC, and 475CFC by annealing at temperatures of 350°C, 400°C, 425°C, 450°C, and 475°C. RISE analysis of CFCs can obtain Raman, SEM images, as shown in Figure 3. Red, blue, green, purple, and yellow represent high-G/D, medium-G/D, low-G/D, background, and fluorescent areas, respectively. RISE reveals the change of G-band and D-band of CFC under different treatment conditions. It can be seen from Figure 3c–h that the red area gradually disappears with the increase of annealing temperature, which proves that the order degree of CFC is reduced due to the activation process and defects are introduced on the surface. Combined with other characterization methods, such as BET, contact angle, and other experiments, the relationship between the electrochemical properties and structures of different activated electrodes was proved.

4.2 | In situ electrochemical Raman spectroscopy

In situ studies do not refer to a specific research means or methods; it is the change of research methods. The traditional method (off-line) is to isolate the research object from the change system and then analyze the change results. This method cannot analyze the changes of the research object in time and can only obtain some static results. In situ research, the analyzer is directly connected to the changing electrode without changing the working state of the electrode so as to acquire real and accurate results. In situ electrochemical Raman spectroscopy has an important application in the identification of molecules involved with the electrochemical processes, including intermediate phases, providing intuitive information on the microstructure of electrode surface/interface during the battery charging and discharging.

An in situ Raman cell was designed by Hu et al.[85] as Figure 4a. Li metal as the anode, poly (methacrylate)/poly (ethylene glycol)-$LiClO_4$-3wt%SiO_2 composite polymer electrolyte (CPE) and multiwall carbon nanotubes (CNTs) as cathode. CO_2 reaches the cathode through the intake hole to participate in the reaction, and the excess gas is excluded from the outlet. A small hole is cut in the top of the cathode shell and protected with optical glass to allow the laser signal to reach the cathode. Raman spectroscopy was used to analyze cathode at different potentials (different charging and discharging states of the same electrode) as Figure 4c. During the discharge process, the Li anode loses electrons and releases Li^+ to the cathode, thus causing CO_2 molecules to react with Li^+. Raman spectroscopy (red line) showed that the Raman peak of Li_2CO_3 increased gradually (located at 1,090 cm^{-1}) with the deepening of discharge degree. This result proves that Li^+ reacts with CO_2 to produce Li_2CO_3 during the discharge. In the charging process, the peak of Li_2CO_3 gradually weakens, representing the decomposition of Li_2CO_3. There are no other Raman peaks found on the Raman spectrum, indicating that no other side effects occurred during charging and discharging. XRD is used to analyze the cathode after charging and discharging, which further proves that the discharge product is Li_2CO_3 as Figure 4b. All of these results to verify the reaction mechanism of Li-CO_2 battery: $4Li + 3CO_2 \leftrightarrow 2Li_2CO_3 + C$.

Yang et al. studied the conversion-intercalation process of LiCl and LiBr in graphite by in situ Raman spectroscopy.[86] $(LiBr)_{0.5}(LiCl)_{0.5}$–graphite and graphite as cathode and anode, respectively. LiTFSI, LiOTf, and polyvinyl alcohol are mixed as electrolyte. The $(LiBr)_{0.5}(LiCl)_{0.5}$–graphite electrode experiences a two-step reaction during charging. When the charging voltage is 4.0–4.2 V, Br^- is oxidized to Br^0 and intercalate into graphite to generate $C_n[Br]$. The reaction equation is as follows:

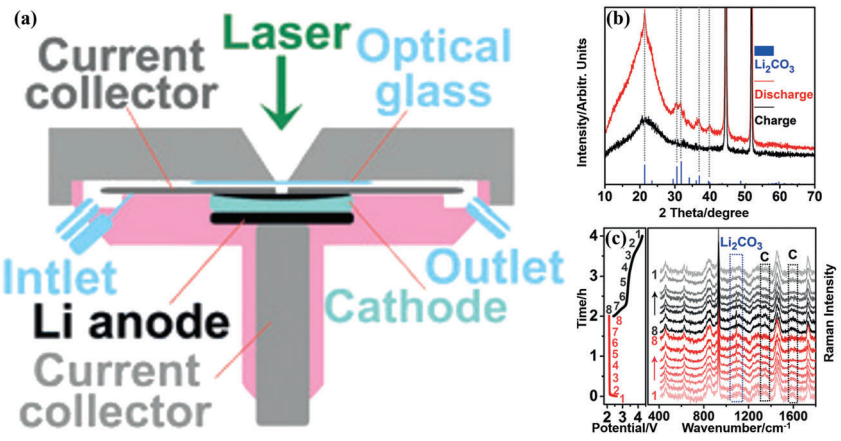

FIGURE 4 (a) Design of the in-situ Raman cell; (b) XRD patterns of the cathode after discharge and recharge; (c) discharge/charge profiles with 16 selected states and the corresponding in situ Raman spectra. This figure was reprinted with permission from Hu et al.[85] Copyright 2017 John Wiley & Sons ltd [Colour figure can be viewed at wileyonlinelibrary.com]

$$LiBr + C_n \leftrightarrow C_n[Br] + Li^+ + e^-$$

When the charging voltage is 4.2–4.5 V, Cl^- is oxidized to Cl^0 and intercalate into graphite to generate $C_n[BrCl]$. The reaction equation is as follows:

$$LiCl + C_n[Br] \leftrightarrow C_n[BrCl] + Li^+ + e^-$$

There are two pairs of redox peaks on the cathode cyclic voltammetry curve, corresponding to the two-step reaction of Br^- and Cl^-. In situ Raman spectral analysis was performed on the cathode electrodes under different charging/discharging states. There is no Raman peak of Br_2 when charging 0%. When charging gradually increases to 50%, the Raman peak of Br_2 at 242 cm^{-1} gradually strengthens, which proves the intercalation process of Br_2 in charging process. When charging to 75%, Raman peak of BrCl at 310 cm^{-1} was observed, but no Raman peak of Cl_2 was observed before, proving that Cl^- conversion-intercalation process occurred after Br^- conversion-intercalation process and Cl^- combines with $C_n[Br]$ to form $C_n[BrCl]$ with the Br_2 peak weakens. This result is consistent with the results of galvanostatic discharge-charge test. After charging to 100%, the Raman peak of Br_2 completely disappears, and the peak of BrCl is enhanced, proving that the Cl^- completely combine with the previous $C_n[Br]$ to generate $C_n[BrCl]$. In this work, the conversion-intercalation mechanism of Cl^- and Br^- in graphite was strongly proved by the combination of in situ electrochemical Raman spectroscopy. Laura et al.[87] used in situ Raman spectroscopy to study the charging/discharging process of carbon-coated $ZnFe_2O_4$ anode in a lithium-sulfur battery. It proves that the lithium removal process is not completely reversible and parts of lithium remains being trapped in the carbon shell. Xie et al.[88] used in situ electrochemical Raman spectroscopy to track the changes in the signals of Polysulfide intermediates as the voltages ranged from 2.7 to 1.8 V. The sulfur chain signals of different polysulfide species were studied in order to understand the morphological evolution of sulfur during the charge and discharge. Zhong et al.[89] investigated the mechanism of titanium substitution for P2–$Na_{2/3}Ni_{1/3}Mn_{2/3}O_2$ and P2–$Na_{2/3}Ni_{1/3}Mn_{1/3}Ti_{1/3}O_2$ cathode in sodium ion batteries. Indeed, in situ Raman spectroscopy plays an important role in characterizing the evolution of electrode materials and understanding the energy storage mechanism of electrodes in both lithium-ion and sodium-ion batteries. Such in situ Raman spectroscopy technique can also gain mechanistic insight into some electrocatalysis processes. Leyva-Garcia et al.[90] used in situ Raman spectroscopy to analyze the interaction between two kinds of activated carbon materials (ANK-3 and MWV-E510A) and hydrogen in an electrochemical hydrogen storage process at cathode. The C–H bond appears at 0.69 and 0.59 V for these two types of carbon respectively, indicating that MWVE-510A is more prone to store hydrogen.

4.3 | Electrochemical tip-enhanced Raman spectroscopy

Electrochemical tip enhanced Raman spectroscopy (EC-TERS) combines electrochemistry with tip enhanced Raman spectroscopy. As a kind of optical technology with high spatial resolution, TERS can provide the chemical composition information of substances.[91] This technique is particularly suitable for surface/interface studies due to the electromagnetic coupling enhancement decays exponentially with the distance between the tip and the sample. In the latest report of Hou research group, the combination of STM-AFM-TERS not only determines the structural and chemical heterogeneity among three pentacene species but also proves the importance of specific local interactions between pentacene and Ag(110) surfaces.[92] In the electrochemical process, the change of electrode potential (i.e., the Fermi level of the electrode) will cause the change of interface structure. Once the potential control or electrolyte is disconnected, the interface process will change, and the interface structure may change to an open circuit potential state, which is different from the electrode state during charge and discharge. Therefore, it is very necessary to combine the TERS method with electrochemical characterization. In situ studies with high sensitivity and spatial resolution can be realized by EC-TERS to obtain the structural information of materials in the electrochemical reaction process. TERS and SERS (Surface enhanced Raman spectroscopy) has the same enhancement mechanism. The TERS replaced multiple SERS hot spots with hot spots formed by Au or Ag tips controlled by scanning probe microscopy, depending on light enhancement and space constraints near the plasma nanotips. The plasma nanotips can be positioned on the sample and controlled by a suitable scanning probe microscope (such as atomic force microscope [AFM] or scanning tunneling microscope [STM]).[93] Through the raster scan of nanotips, it can obtain high spatial resolution of nanometer images. The structure diagram of EC-TERS is shown in Figure 5a. The electronic part is the same as EC-STM, where the potential of the tip (WE1) and substrate (WE2) is controlled by a double potentiostat. The laser is introduced horizontally into the electrochemical cell through a long working range microscope objective (NA = 0.45). By tilting the single crystal to about 10°, the laser can be correctly

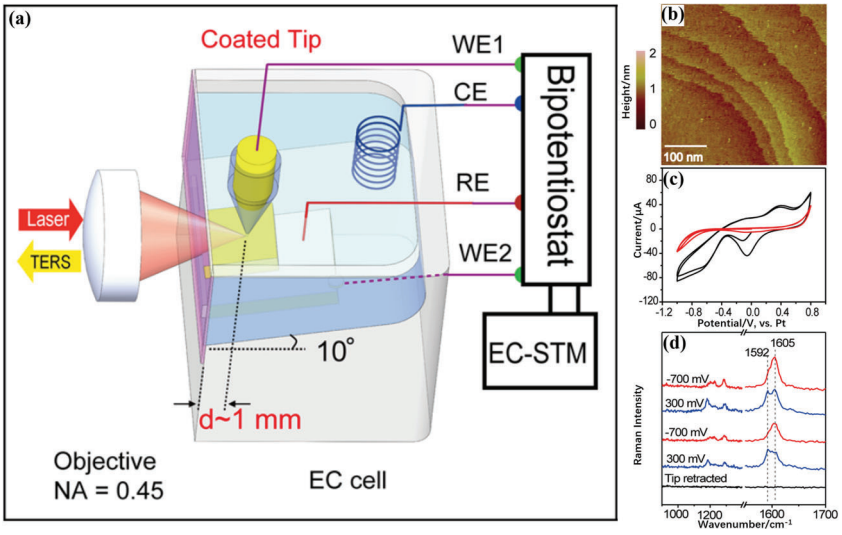

FIGURE 5 (a) Structure diagram of EC-TERS; (b) STM image of 4-PBT/au(111); (c) cyclic voltammetry curves of 4-PBT/au(111) and au(111); (d) EC-TERS spectra of 4-PBT/au (111). This figure was reprinted with permission from Zeng et al.[94] Copyright 2015 American Chemical Society [Colour figure can be viewed at wileyonlinelibrary.com]

focused on the tip to efficiently collect the Raman signal. The generated TERS signal is collected by the same target and sent to Raman system for detection.

Zeng et al.[94] used EC-TERS technology to study the performance of 4-PBT/Au(111) (4′-(pyridin-4-yl)biphenyl-4-yl)methanethiol is attached to Au(111)) electrode, 0.1 M $NaClO_4$ as the electrolyte. The STM image of 4-PBT/Au (111) is shown in Figure 5b, showing a clear ladder on the surface of the single crystal. 4-PBT molecule forms a dense self-assembled monolayer on the surface of gold through gold-sulfur bonds and has few surface defects. The cyclic voltammetry (CV) of 4-PBT/Au(111) and Au(111) is shown in the red and black curves in Figure 5c. The CV curve has a wide potential window (0.7 $\sim$ +0.3 V). In contrast, the surface of Au(111) exhibits complex electrochemical processes under potential window, due to the passivation of the surface by 4-PBT molecules. The Raman spectra of 4-PBT/Au(111) at different potentials were shown in Figure 5d. Double peaks could be observed at 1,592 and 1,605 cm^{-1} on 0.3 V. When the voltage was 0.7 V, the low-wavenumber peak disappeared and only one shoulder peak appeared. This special Raman peak transformation was not observed in EC-SERS system. This advanced Raman characterization technique combines the advantages of electrochemistry, STM and Raman, which has great advantages for the study of carbon-based electrode materials.

5 | SUMMARY AND PERSPECTIVES

Carbon materials are very common as electrode active materials for supercapacitors and lithium-ion batteries. Analysis of the structural features of carbon materials can establish the immediate relationship between the structure and performance. Raman spectroscopy, as the molecular spectroscopy technique, has been well developed for the structural characterization of carbon materials. Amounts of information can be obtained from the shape, position, and strength of the Raman spectrum peak. In this review, the Raman spectra data of carbon materials with electrical double layer energy storage mechanism and intercalation/de-intercalation energy storage mechanism are summarized. And the relevant examples were given to analyze the Raman spectra effectively. The structural information obtained by the Raman spectroscopy is of great significance for the optimization of electrode materials and the deep understanding of the energy storage mechanism of electrode materials. At the same time, we also introduce several advanced correlative-Raman technologies. RISE can obtain the surface morphology and structural information of the same micro-region. In situ electrochemical Raman spectroscopy can clarify Raman information in the electrode reaction process. EC-TERS can realize the integration of morphology, structural, and electrochemical information.

Although Raman spectroscopy has been widely used to study carbon-based electrode materials, there are still some challenges. A single Raman spectrum can only obtain information related to molecular energy level structure, which is simple. This article only introduces a few correlative-Raman technologies, and there are some other correlative-Raman technologies, such as Fourier transform infrared (FTIR) and Raman spectroscopy can be combined to provide complementary information. The integration of Raman and photoluminescence spectrometer can simultaneously characterize the vibrational and electronic properties of samples in the same instrument platform, although some of these techniques have not yet been applied to the research field of carbon-based energy storage electrodes. However, in the future, they will be

an effective method for the study of electrode materials due to their unique advantages.

ACKNOWLEDGMENTS

This research was supported by the National Natural Science Foundation of China (51932003 and 51872115), the 2020 International Cooperation Project of the Department of Science and Technology of Jilin Province (20200801001GH), the Program for the Development of Science and Technology of Jilin Province (20190201309JC), Project for Self-innovation Capability Construction of Jilin Province Development and Reform Commission (2021C026), National Postdoctoral Program for Innovative Talents (BX20200147), China Postdoctoral Science Foundation (2020M670838), the Jilin Province/Jilin University Co-construction Project Funds for New Materials (SXGJSF2017-3, Branch-2/440050316A36), the Open Project Program of Wuhan National Laboratory for Optoelectronics of 2018WNLOKF022, the Fundamental Research Funds for the Central Universities (Jilin University), and the "Double-First Class" Discipline for Materials Science & Engineering.

ORCID

Wei Zhang https://orcid.org/0000-0002-6414-7015

REFERENCES

[1] M. D. Stoller, S. Park, Y. Zhu, J. An, R. S. Ruoff, *Nano Lett.* **2009**, *8*, 3498.
[2] E. E. Storey, A. S. Helmy, *J Raman Spectrosc* **2019**, *50*, 958.
[3] L. Avram, A. Stefancu, D. Crisan, N. Leopold, V. Donca, E. Buzdugan, R. Craciun, D. Andras, I. Coman, *Exp. Ther. Med.* **2020**, *20*, 213.
[4] Z. Bo, J. Yang, H. Qi, J. Yan, K. Cen, Z. Han, *Energy Storage Materials* **2020**, *31*, 64.
[5] H. G. M. Edwards, J. M. Chalmers, *Antiquity* **2005**, *37*, 958.
[6] S. M. Dresselhaus, A. Jorio, M. Hofmann, G. Dresselhaus, R. Saito, *Nano Lett.* **2010**, *10*, 751.
[7] S. Sil, N. Kuhar, S. Acharya, S. Umapathy, *Sci. Rep.* **2013**, *391*, 1813.
[8] M. S. Dresselhaus, A. Jorio, R. Saito, *Annu. Rev. Condens. Matter Phys* **2010**, *1*, 89.
[9] S. Webster, D. A. Smith, D. N. Batchelder, *Vib. Spectrosc.* **1998**, *18*, 51.
[10] J. Wang, J. Tu, H. Lei, H. Zhu, *RSC Adv.* **2019**, *9*, 38990.
[11] P. Selvarajan, G. Chandra, S. Bhattacharya, S. Sil, A. Vinu, S. Umapathy, *Emergent Materials* **2019**, *2*, 417.
[12] Y. Qiao, J. Yi, S. Guo, Y. Sun, S. Wu, X. Liu, S. Yang, P. He, H. Zhou, *Energy Environ. Sci.* **2018**, *11*, 1211.
[13] N. Sinan, E. Unur, *Mater. Chem. Phys.* **2016**, *183*, 571.
[14] S. Li, Y. Dong, J. Zhou, Y. Liu, J. Wang, X. Gao, Y. Han, P. Qi, B. Wang, *Energy Environ. Sci.* **2018**, *11*, 1318.
[15] C. Wang, Q. Zhang, X. Zhang, X.-G. Wang, Z. Xie, Z. Zhou, *Small* **2018**, *14*, e1800641.
[16] W. Zhang, D. Wang, W. Zheng, *J. Energy Chem.* **2020**, *41*, 100.
[17] P. Simon, Y. Gogotsi, *Nat. Mater.* **2008**, *7*, 845.
[18] Y. Wen, K. He, Y. Zhu, F. Han, Y. Xu, I. Matsuda, Y. Ishii, J. Cumings, C. Wang, *Nat. Commun.* **2014**, *5*, 4033.
[19] G. Wang, H. Wang, X. Lu, Y. Ling, M. Yu, T. Zhai, Y. Tong, Y. Li, *Adv. Mater.* **2014**, *26*, 2676.
[20] W. Y. Tsai, P. L. Taberna, P. Simon, *J. am. Chem. Soc.* **2014**, *136*, 8722.
[21] J. Chmiola, G. Yushin, Y. Gogotsi, C. Portet, P. Simon, P. L. Taberna, *Science* **2006**, *313*, 1760.
[22] H. J. Liu, J. Wang, C. X. Wang, Y. Y. Xia, *Adv. Energy Mater.* **2011**, *1*, 1101.
[23] X. Y. Chu, F. L. Meng, T. Deng, Y. Lu, O. Bondarchuk, M. L. Sui, M. Feng, H. B. Li, W. Zhang, *Nanoscale* **2020**, *12*, 5669.
[24] M. Lu, W. Han, H. Li, W. Shi, J. Wang, B. Zhang, Y. Zhou, H. Li, W. Zhang, W. Zheng, *Energy Stor. Mater.* **2019**, *16*, 163.
[25] J. Hazekamp, M. G. Reed, C. V. Howard, A. A. V. Apeldoorn, C. Ottto, *J. Microsc.* **2011**, *244*, 122.
[26] C. Cardell, I. Guerra, *Trends Analyt Chem* **2016**, *77*, 156.
[27] P. Verma, *Chem. Rev.* **2017**, *117*, 6447.
[28] T. Yano, T. Ichimura, S. Kuwahara, F. H'Dhili, K. Uetsuki, Y. Okuno, P. Verma, S. Kawata, *Nat. Commun.* **2013**, *4*, 1.
[29] D. Wang, W. Zhang, N. E. Drewett, X. Li, S. J. Yoo, S. G. Lee, J. G. Kim, T. Deng, X. Zhang, X. Shi, W. Zheng, *ACS Cent. Sci.* **2018**, *4*, 81.
[30] X. Dong, H. Yu, Y. Ma, J. L. Bao, D. G. Truhlar, Y. Wang, Y. Xia, *Proc. Natl. Acad. Sci. U. S. a.* **2017**, *23*, 2560.
[31] A. Smekal, *Naturwissenschaften* **1923**, *11*, 873.
[32] A. G. Shenstone, *Nature* **1928**, *121*, 3175.
[33] C. V. Raman, K. S. Krishnan, *Nature* **1928**, *121*, 3048.
[34] H. K. Mieda, A. A. Mamun, T. Ogura, T. Kitagawa, P. M. Kozlowski, *J. Raman Spectrosc.* **2020**, *51*, 1331.
[35] P. Saha, B. Ghosh, A. Mazumder, G. D. Mukherjee, *Mater. Res. Express.* **2020**, *7*, 025902.
[36] Y. Ozaki, A. Mizuno, H. Sato, K. Kawauchi, S. Muraishi, *Appl. Spectrosc.* **2016**, *46*, 533.
[37] Q. Li, J. Zhang, D. Shi, X. Li, Q. Liu, *Anal. Methods* **2016**, *8*, 5448.
[38] S. A. Majeed, *Analyst* **2020**, *145*, 6744.
[39] C. S. Casari, *Istituto Lombardo-Accademia di Scienze e Lettere-Rendiconti di Scienze* **2012**, *146*, 17.
[40] M. Acik, Y. J. Chabal, *Jpn. J. Appl. Phys.* **2011**, *50*, 070101.
[41] M. Lazzeri, C. Attaccalite, L. Wirtz, F. Mauri, *Phys. Rev. B* **2008**, *78*, 1.
[42] L. M. Malard, M. A. Pimenta, G. Dresselhaus, M. S. Dresselhaus, *Phys. Rep.* **2009**, *473*, 51.
[43] I. A. Rodríguez-Pérez, L. Zhang, J. M. Wrogemann, D. M. Driscoll, M. L. Sushko, K. S. Han, J. L. Fulton, M. H. Engelhard, M. Balasubramanian, V. V. Viswanathan, V. Murugesan, X. Li, D. Reed, V. Sprenkle, M. Winter, T. Placke, *Adv. Energy Mater.* **2020**, *10*, 2001256.
[44] J. M. Wrogemann, S. Künne, A. Heckmann, I. A. Rodríguez-Pérez, V. Siozios, B. Yan, J. Li, M. Winter, K. Beltrop, T. Placke, *Adv. Energy Mater.* **2020**, *10*, 1902709.
[45] Z. Zhang, Q. Zhang, Y. Chen, J. Bao, X. Zhou, Z. Xie, J. Wei, Z. Zhou, *Angew. Chem., Int. Ed.* **2015**, *54*, 6550.
[46] X. Zhang, Q. Zhang, Z. Zhang, Y. Chen, Z. Xie, J. Wei, Z. Zhou, *Chem. Commun.* **2015**, *51*, 14636.
[47] M. Zhi, F. Yang, F. Meng, M. Li, A. Manivannan, N. Wu, *ACS Sustainable Chem. Eng.* **2014**, *2*, 1592.
[48] R. L. McCreery, *Chem. Rev.* **2008**, *108*, 2646.

[49] L. L. Zhang, X. S. Zhao, *Chem. Soc. Rev.* **2009**, *38*, 2520.
[50] H. Jeon, J. M. Jeong, S. B. Hong, M. Yang, J. Park, D. H. Kim, S. Y. Hang, B. G. Choi, *Electrochim. Acta* **2018**, *280*, 9.
[51] L. G. Cancado, A. Jorio, E. H. Ferreira, F. Stavale, C. A. Achete, R. B. Capaz, M. V. Moutinho, A. Lombardo, T. S. Kulmala, A. C. Ferrari, *Nano Lett.* **2011**, *11*, 3190.
[52] A. Ferrari, J. Robertson, *Phys. Rev. B* **2000**, *61*, 14095.
[53] J. Chen, Y. Han, X. Kong, X. Deng, H. J. Park, Y. Guo, S. Jin, Z. Qi, Z. Lee, Z. Qiao, R. S. Ruoff, H. Ji, *Angew. Chem., Int. Ed.* **2016**, *55*, 13822.
[54] H. Wang, J. Deng, C. Xu, Y. Chen, F. Xu, J. Wang, Y. Wang, *Energy Stor. Mater.* **2017**, *7*, 216.
[55] D. Chen, G. Ji, Y. Ma, J. Y. Lee, J. Lu, *ACS Appl. Mater. Interfaces* **2011**, *3*, 3078.
[56] W. Huang, X. Xiao, C. Engelbrekt, M. Zhang, S. Li, J. Ulstrup, L. Ci, J. Feng, P. Si, Q. Chi, *Mater. Chem. Front.* **2017**, *1*, 1185.
[57] X. Wang, K. Chen, G. Wang, X. Liu, H. Wang, *ACS Nano* **2017**, *11*, 11602.
[58] M. Chen, J. Liu, D. Chao, J. Wang, J. Yin, J. Lin, H. Jin Fan, Z. Xiang Shen, *Nano Energy* **2014**, *9*, 364.
[59] M. Guo, J. Balamurugan, X. Li, N. H. Kim, J. H. Lee, *Small* **2017**, *13*, 1701275.
[60] M. Wang, Y. Tang, *Adv. Energy Mater.* **2018**, *8*, 1703320.
[61] H. Yang, T. Qin, T. Deng, W. Zhang, W. Zheng, *Energy Fuels* **2020**, *34*, 15701.
[62] X. Shi, W. Zhang, J. Wang, W. Zheng, K. Huang, H. Zhang, S. Feng, H. Chen, *Adv. Energy Mater.* **2016**, *6*, 1601378.
[63] M. S. Dresselhaus, G. Dresselhaus, *Adv. Math. Phys.* **2002**, *51*, 1.
[64] T. Placke, G. Schmuelling, R. Kloepsch, P. Meister, O. Fromm, P. Hilbig, H. W. Meyer, M. Winter, *Z Anorg Allg Chem* **2014**, *640*, 1996.
[65] E. Gey, *Z Phys Chem (N F)* **1991**, *174*, 226.
[66] J. Xu, Y. Dou, Z. Wei, J. Ma, Y. Deng, Y. Li, H. Liu, S. Dou, *Adv. Sci.* **2017**, *4*, 1700146.
[67] A. Das, B. Chakraborty, S. Piscanec, S. Pisana, A. K. Sood, *Rev. B* **2009**, *79*, 1.
[68] S. Pisana, M. Lazzeri, C. Casiraghi, K. S. Novoselov, A. K. Geim, A. C. Ferrari, F. Mauri, *Nat. Mater.* **2007**, *6*, 198.
[69] J. C. Chacon-Torres, L. Wirtz, T. Pichler, *ACS Nano* **2013**, *7*, 9249.
[70] E. Gey, *Zeitschrift für Physikalische Chemie* **1991**, *174*, 226.
[71] C. Sole, N. E. Drewett, L. J. Hardwick, *Faraday Discuss.* **2014**, *172*, 223.
[72] M. Angell, C. J. Pan, Y. Rong, C. Yuan, M. C. Lin, B. J. Hwang, H. Dai, *Proc. Natl. Acad. Sci. U. S. a.* **2017**, *114*, 834.
[73] X. Shi, T. Deng, B. Zhang, W. Zhang, L. Sui, H. Yang, D. Wang, W. Shi, C. M. Chen, W. Zheng, *ChemElectroChem* **2017**, *4*, 3238.
[74] K. Kim, Q. Guo, J. Razink, M. M. Lerner, C. Fang, X. Ji, *Angew. Chem., Int. Ed.* **2020**, *59*, 19924.
[75] H. Zhang, X. Liu, B. Qin, S. Passerini, *J. Power Sources* **2020**, *449*, 227594.
[76] A. M. Saitta, M. Lazzeri, M. Calandra, F. Mauri, *Phys. Rev. Lett.* **2008**, *100*, 226401.
[77] E. Zhang, W. Cao, B. Wang, X. Yu, L. Wang, Z. Xu, B. Lu, *Energy Stor. Mater.* **2018**, *11*, 91.
[78] J. Gao, S. Tian, L. Qi, H. Wang, *Electrochim. Acta* **2015**, *176*, 22.
[79] J. A. Seela, J. R. Dahn, *J. Electrochem. Soc.* **2000**, *147*, 892.
[80] P. A. Walker, W. K. Kowalchyk, M. D. Morris, *Anal. Chem.* **1995**, *67*, 4255.
[81] O. Hollricher, U. Schmidt, S. Breuninger, *Microscopy Today* **2014**, *22*, 36.
[82] Y. Zheng, T. Deng, W. Zhang, W. Zheng, *J. Energy Chem.* **2020**, *47*, 210.
[83] R. Schmidt, H. Fitzek, M. Nachtnebel, C. Mayrhofer, H. Schroettner, A. Zankel, *Macromol. Symp.* **2019**, *384*, 1800237.
[84] S. Liu, B. Yu, H. Jing, Z. Zhao, H. Liu, L. Yao, W. Zhang, *Surface Technology* **2021**, *50*, 28.
[85] X. Hu, Z. Li, J. Chen, *Angew. Chem., Int. Ed.* **2017**, *56*, 5785.
[86] C. Yang, J. Chen, X. Ji, T. P. Pollard, X. Lü, C.-J. Sun, S. Hou, Q. Liu, C. Liu, T. Qing, Y. Wang, O. Borodin, Y. Ren, K. Xu, C. Wang, *Nature* **2019**, *569*, 245.
[87] C. F. Laura, M. Franziska, P. Stefano, J. Laurence, J. Hardwick, *Chem. Commun.* **2016**, *52*, 3970.
[88] J. Xie, Y. W. Song, B. Q. Li, H. J. Peng, J. Q. Huang, Q. Zhang, *Angew. Chem., Int. Ed.* **2020**, *59*, 22150.
[89] X. B. Zhong, C. He, F. Gao, Z. Q. Tian, J. F. Li, *J. Energy Chem.* **2021**, *53*, 323.
[90] S. Leyva-García, E. Morallón, D. Cazorla-Amorós, F. Béguin, D. Lozano-Castelló, *Carbon* **2014**, *69*, 401.
[91] J. H. K. Pfisterer, K. F. Domke, *Curr. Opin. Electrochem.* **2018**, *8*, 96.
[92] J. Xu, X. Zhu, S. Tan, Y. Zhang, B. Li, Y. Tian, H. Shan, X. Cui, A. Zhao, Z. Dong, J. Yang, Y. Luo, B. Wang, J. G. Hou, *Science* **2021**, *371*, 818.
[93] T. Ouyang, K. Cheng, F. Yang, J. Jiang, J. Yan, K. Zhu, K. Ye, G. Wang, L. Zhou, D. X. Cao, *Chem. Eng. J.* **2017**, *335*, 638.
[94] Z. C. Zeng, S. C. Huang, D. Y. Wu, L. Y. Meng, M. H. Li, T. X. Huang, J. H. Zhong, X. Wang, Z. L. Yang, B. Ren, *J. am. Chem. Soc.* **2015**, *137*, 11928.

SUPPORTING INFORMATION

Additional supporting information may be found online in the Supporting Information section at the end of this article.

How to cite this article: Y. Zheng, T. Deng, N. Yue, W. Zhang, X. Zhu, H. Yang, X. Chu, W. Zheng, *J Raman Spectrosc* **2021**, 1. https://doi.org/10.1002/jrs.6178